Physicochemical Study of Spiropyran-terthiophene Derivatives: Photochemistry and Thermodynamics

Michele Zanoni[a], Simon Coleman[a], Kevin J. Fraser[a], Robert Byrne[a], Klaudia Wagner[b], Sanjeev Gambhir[b], David L. Officer[b], Gordon G. Wallace[b] and Dermot Diamond[a]

Received (in XXX, XXX) Xth XXXXXXXXX 20XX, Accepted Xth XXXXXXXXX 20XX
DOI: 10.1039/b000000x

The photochemistry and thermodynamics of two terthiophene (**TTh**) derivatives bearing benzospiropyran (**BSP**) moieties, 1-(3,3''-dimethylindoline-6'-nitrobenzospiropyranyl)-2-ethyl 4,4''-didecyloxy-2,2':5',2''-terthiophene-3'-acetate (**BSP-2**) and 1-(3,3''-dimethylindoline-6'-nitrobenzospiropyranyl)-2-ethyl 4,4''-didecyloxy-2,2':5',2''-terthiophene-3'-carboxylate (**BSP-3**), differing only by a single methylene spacer unit, have been studied. The kinetics of photogeneration of the equivalent merocyanine (**MC**) isomers (**MC-2** and **MC-3**, respectively), the isomerisation properties of **MC-2** and **MC-3**, and the thermodynamic parameters have been studied in acetonitrile, and compared to the parent, non-**TTh**-functionalised, benzospiropyran derivative, **BSP-1**. Despite the close structural similarity of **BSP-2** and **BSP-3**, their physicochemical properties were found to differ significantly; examples include activation energies ($E_{a(MC\text{-}2)}$ = 75.05 KJ mol^{-1}, $E_{a(MC\text{-}3)}$ = 100.39 kJ mol^{-1}) and entropies of activation ($\Delta S^{\ddagger}_{MC\text{-}2}$ = -43.38 J K^{-1} mol^{-1}, $\Delta S^{\ddagger}_{MC\text{-}3}$ = 37.78 J K^{-1} mol^{-1}) for the thermal relaxation from **MC** to **BSP**, with the **MC-3** value much closer to the unmodified **MC-1** value (46.48 J K^{-1} mol^{-1}) for this latter quantity. The thermal relaxation kinetics and solvatochromic behaviour of the derivatives in a range of solvents of differing polarity (ethanol, dichloromethane, acetone, toluene and diethyl ether) are also presented. Differences in the estimated values of these thermodynamic and kinetic parameters are discussed with reference to the molecular structure of the derivatives.

Introduction

Nitrobenzospiropyran (**BSP**) is member of a family of photo/thermochromic molecules that have been widely studied due to their ability to be switched reversibly under various external stimuli between two molecular states that exhibit dramatically different properties.[1-22] This behaviour has attracted great interest in terms of possible applications such as optical memory[12], biomaterials for targeted therapeutic agents8, components for ophthalmic lenses[9], molecular functionalization of micro channels and as optical probes for the analysis of nano-structures in ionic liquids (**ILs**).[14]

Photochromism is a phenomenon that occurs when electromagnetic radiation is absorbed by a molecule that undergoes a reversible rearrangement between two forms, such as 1-(2-hydroxyethyl)-3,3-dimethylindoline-6'-nitrobenzospiropyran (**BSP-1**, Figure 1)1-13 and its equivalent merocyanine form (**MC-1**), with dramatic accompanying changes in the absorption spectra in the visible region.[13]

Benzospiropyran is a molecule that exists as two heterocyclic functional units connected by a tetrahedral sp3 hybridised carbon atom. This atom co-joins two orthogonal planes comprising an indoline subunit and a benzopyran subunit, the common component for all the spiropyran moieties.

Photo-induced isomerisation processes are well known in the literature.[6, 7, 18-21] In spiropyrans, heterocyclic ring cleavage occurs at the C_{spiro}-O bond when exposed to UV light[6, 13], leading to the formation of the merocyanine (**MC**) species that can be detected via a striking colour change due to the strong absorbance of the **MC** isomer in the visible region (Figure 1). Upon irradiation with white light, the system reverts back to the original **BSP** form. The **MC** isomer absorbance is sensitive to its immediate molecular environment, leading to solvent dependant colour changes, and the solvent can also mediate the equilibrium between the isomers.

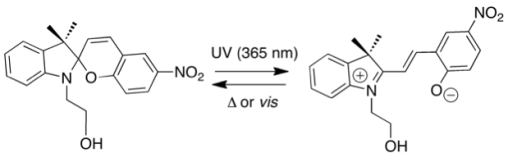

BSP-1 **MC-1**

Fig. 1 Molecular structure and isomerisation of 1-(2-hydroxyethyl)-3,3-dimethylindoline-6'-nitrobenzospiropyran (**BSP-1**) spiropyran.

The solvatochromism of various benzospiropyran derivatives has been reported previously including nitro- and methoxy-substituted spiro-moieties.[16, 17, 22] Recently, the well-known photo-, thermo- and solvato-chromic properties of benzospiropyran (**BSP**) and spirooxazine derivatives have been used by our group to provide new insights into the nanostructure of ILs through in-situ mediation of their switching behaviour.[16, 17] Furthermore the presence of the phenolate anion in the **MC** isomer provides a weak binding capacity for certain metal ions (d- and f- elements), and the resulting complexes generate new absorbance bands in the visible region, which are directly influenced by the type of metal ion present.[18-21]

Polythiophenes (**PThs**) are a class of organic polymeric semiconductors with extremely interesting conductivity, electrochromism and electroluminescence[23] properties, which have been explored for applications such as electrochemical sensors and energy harvesting devices.[24-27] From a materials chemistry perspective, they are particularly attractive due to their high chemical stability and relative ease of isolation.[25] Other interesting **pTh** properties previously reported in the literature include thermochromism, ionochromism, photochromism and bio-chromism.[24-37] Chromic variations are generated by

conformational changes or folding of the polymer chains, with consequent dramatic variation in the conjugation length of the whole system, which can be monitored using spectroscopy. Substituents connected to the three-aromatic rings backbone can have a considerable effect on the overall conjugation of the system, influencing the properties and the distribution of the π-electrons in the structure.

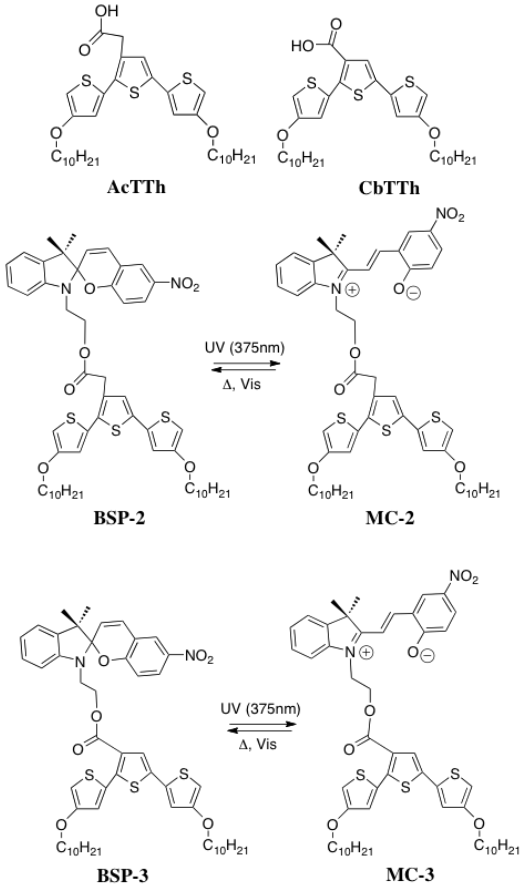

Fig. 2 Structures of the **TTh** and **TTh-BSP** derivatives studied: Methyl 4,4''-didecyloxy-2,2':5',2''-terthiophene-3'-acetate (**AcTTh**); 4,4''-didecyloxy-2,2':5',2''-terthiophene-3'-carboxylic acid (**cbTTh**); 1-(3,3''-dimethylindoline-6'-nitrobenzospiropyranyl)-2-ethyl 4,4''-didecyloxy-2,2':5',2''-terthiophene-3'-acetate (**BSP-2**) and 1-(3,3''-dimethylindoline-6'-nitrobenzospiropyranyl)-2-ethyl 4,4''-didecyloxy-2,2':5',2''-terthiophene-3'-carboxylate (**BSP-3**).

As part of our ongoing interest in functionalised **PThs**, we recently reported the first synthesis of a **BSP**-functionalised poly(terthiophene) and undertook a detailed study of its complex electrochemical and photochemical properties.[38] The **BSP** was attached to the terthiophene monomer (**acTTh**, Figure 2) by an acetate linkage (**BSP-2**, Figure 2). Given the multiple effects of the spiropyran on the electrochemical behaviour of the poly(terthiophene), we were interested in how these might vary depending on the distance of the spiropyran from the polymer backbone. Therefore, we synthesised the **BSP**-terthiophene monomer in which the ester linkage was directly attached to the terthiophene moiety (**BSP-3**, Figure 2), differing from **BSP-2** only by one carbon atom. Prior to studying its electrochemical polymerisation and resulting polymer properties, we deemed it important to determine the photochemical properties of **BSP-3** and compare them to **BSP-1** and **BSP-2**.

Therefore, in this work, the photochemical behaviour of the two **BSP**-functionalised terthiophene monomers, 1-(3,3''-dimethylindoline-6'-nitrobenzospiropyranyl)-2-ethyl 4,4''-didecyloxy-2,2':5',2''-terthiophene-3'-acetate (**BSP-2**) and 1-(3,3''-dimethylindoline-6'-nitrobenzospiropyranyl)-2-ethyl 4,4''-didecyloxy-2,2':5',2''-terthiophene-3'-carboxylate (**BSP-3**) is reported, along with a detailed study of the thermodynamics and kinetics of their photo-isomerization. Their photoswitchable behaviour is reported in comparison to the original parent **BSP-1**, as this is important for some innovative applications, such as photo-actuated valves incorporated into micro-fluidic manifolds[11] or light-modulated surfaces for selective cell adhesion/detachment.[39]

Experimental

Materials

1-(2-Hydroxyethyl)-3,3-dimethylindolino-6'-nitrobenzopyrylospiran (**BSP-1**) was purchased from TCI chemicals, Ireland, and was used without further purification. Ethyl (3,3''-dimethylindoline-6'-nitrobenzospiropyranyl)-4,4''-didecyloxy-2,2':5',2''-terthiophene-3'-acetate (**BSP-**2) was synthesised as described previously.[38]

Ethyl (3,3''-dimethylindoline-6'-nitrobenzospiropyranyl)-4,4''-didecyloxy-2,2':5',2''-terthiophene-3'carboxylate (**BSP-**3) was synthesized as follows: 4,4''-Didecyloxy-2,2':5',2''-terthiophene-3'-carboxylic acid (**cbTTh**)[40] **(**0.083 g, 0.138 mmol), dicyclohexylcarbodiimide (DCC) (0.03 g, 0.143 mmol) and 4- dimethylaminopyridine (0.0013 g, 0.011 mmol) were dissolved in DCM (12 ml) at 0 ^{o}C. 1-(2- Hydroxyethyl)-3,3-dimethylindoline-6'-nitrobenzospiropyran **BSP-1** (0.04 g, 0.11 mmol) in DCM (10 ml) was added dropwise over 30 min to the stirring solution. After **BSP-1** was completely added, the reaction mixture was allowed to reach 20 °C. After a further 90 min, 50% of the DCM was removed under reduced pressure, cold ether (10 ml) was added to precipitate the urea salt of DCC. This precipitate was removed by filtration and the filtrate was reduced to give a brown oil, which was purified on a silica column, eluting with DCM. The resulting product was a yellowish-brown oil, which solidified on standing (0.081 g, 77%). After purification via column chromatography, the **BSP-3** was stored in the dark in a sealed glass vial under nitrogen. Characterisation data are available in the ESI section.

The solvents used for the photo- and thermo-chromic analyses (acetonitrile (ACN), ethanol (EtOH), toluene (Tol), acetone (Acet), dichloromethane (DCM) and diethyl ether (DetEth)) were Sigma Aldrich HPLC grade, and used without further purification.

Photochemical Methods

To obtain the rate constants of the ring opening process for **BSP-1**, **BSP-2** and **BSP-3** to their **MC-1**, **MC**-2 and **MC**-3 forms, the derivatives were continuously monitored during UV irradiation at 375 nm. The samples were kept in the dark for 24 hrs to ensure equilibrium in the solvent was reached. Diluted solutions (10^{-4} M) of **BSP-1**, **BSP-2** and **BSP-3** were exposed to UV light and the spectrum of each was taken at intervals from t = 1 minute to t = 45 minutes.

A single exponential model (equation (1)) was used to determine the ring opening rate constants for **BSP-1**, **BSP-2** and **BSP-3**.

$$y = a \times (1 - e^{-(kt)}) + b \quad (1)$$

where **y** is the absorbance at λ_{max} (assumed to be proportional to the concentration of the merocyanime isomer), **a** is a scaling factor, **k** is the first order rate constant (s^{-1}), **b** is the baseline offset and **t** is time (s).

Absorption spectra were recorded using a Perkin Elmer Lambda 900 UV-*Vis*/NIR spectrometer equipped with a thermostatted temperature control system (PTP-1 Peltier System). Photo-conversion of BSP to MC was achieved using an in-house fabricated UV light source consisting of three UV LEDs (Roithner LaserTechnik Gmbh, emission λ_{max} = 375 nm). The LEDs were powered from a 3.75 V current source, which provided an optical power output of 6 mW/cm^2 from each LED. The white light radiation was provided via a DDL 150 W source obtained from Polytec GmbH Waldbronn.

To determine the thermodynamic parameters of the samples and obtain an estimation of the transition state equilibrium of activation ($K^{\ddagger}$) for the **MC→BSP** equilibrium, standard solutions of **BSP-1**, **BSP-2** and **BSP-3** were prepared in concentrations up to 10^{-4} M in acetonitrile. The solutions were stored in volumetric flasks in the dark under nitrogen before the absorbance measurements were acquired. Thermal relaxation analysis of the thermodynamically favoured reversion of **MC** to **BSP** was measured at 5 ^{o}C increments from 283 to 308 K over a period of 1 hour. Samples were irradiated in the dark with the UV-LED system in a sealed quartz cuvette at room temperature for 3 minutes prior to acquisition of the spectra. The study of the **BSP** ⇌ **MC** equilibrium was performed using the LED system in the spectrometer chamber in order to minimise any influence of external light. The **MC→BSP** thermal relaxation typically follows first order kinetics in molecular solvents and the rate is not sensitive to oxygen, but is strongly medium dependent[18-21].

First-order rate constants for the thermal relaxation were determined in this work using Microsoft Excel Solver, by fitting the absorbance data to equation (2), where **y** is the absorbance value at the λ_{max}, **a** is the absorbance at t = 0, **k** is the rate constant, **t** is time and **b** is a baseline offset, as for equation (1)[41].

$$y = ae^{-kt} + b \quad (2)$$

The Arrhenius equation (3) was used to plot the linear temperature dependence of the rate constant for **MC→BSP** thermal relaxation and find the activation energy (E_a) and the pre-exponential factor A.

$$\ln k = E_a / RT + \ln A \quad (3)$$

where **k** = rate constant (s^{-1}), $\mathbf{E_a}$ = Activation energy (kJ mol^{-1}), **R** = gas constant (J mol^{-1} K^{-1}), **T** = temperature (K) and **A** = pre exponential factor (s^{-1})

Following the generalised **BSP** ⇌ **MC** system (Figure 1), the Eyring equation (4) was used to determine the thermodynamic properties at the transition state equilibrium of activation ($K^{\ddagger}$), entropy of activation ($\Delta S^{\ddagger}$), and the enthalpy of activation ($\Delta H^{\ddagger}$). A derivative of this equation, equation (5), can be used to derive the equilibrium of activation ($K^{\ddagger}$)[16, 17, 22]:

$$\ln(k / T) = -\Delta H^{\ddagger} / RT + \ln(k / h) + \Delta S^{\ddagger} / R \quad (4)$$

$$k = (k_B T / h) K^{\ddagger} \quad (5)$$

where **k** = rate constant of the forward reaction, **T** = temperature (K) , $\mathbf{\Delta H^{\ddagger}}$ = enthalpy of activation, $\mathbf{\Delta S^{\ddagger}}$ = entropy of activation, **R** = gas constant, $\mathbf{k_B}$ = Boltzmann constant and **h** = Planck's constant.

Thermodynamic activation properties such as $\Delta S^{\ddagger}$, $\Delta H^{\ddagger}$ and $K^{\ddagger}$ for each **MC** derivative were calculated using the Eyring equation. Equation (6) was used to calculate the Gibbs free energy of activation ($\Delta G^{\ddagger}$).

$$\Delta G^{\ddagger} = \Delta H^{\ddagger} - T\Delta S^{\ddagger} \quad (6)$$

where $\mathbf{\Delta G^{\ddagger}}$ = Gibbs free energy of activation (kJ mol^{-1}), $\mathbf{\Delta H^{\ddagger}}$ = enthalpy of transition state (kJ mol^{-1}), **T** = temperature (K) and $\mathbf{\Delta S^{\ddagger}}$ = entropy of the transition state (J K^{-1} mol^{-1}).

The solvatochromic study was performed at room temperature in 6 different solvent systems (ethanol, toluene, acetone, acetonitrile, diethyl ether and dichloromethane). The solutions (all 10^{-4} M) were sealed and stored under nitrogen overnight before the analysis was performed. Spectra were taken under controlled temperature conditions using the LED system described above to illuminate the samples.

Fluorescence (emission) spectra were recorded with a Perkin Elmer Luminescence Spectrometer LS 50B. Solutions diluted up to 10^{-5} M in acetonitrile of the two freestanding **TTh** molecules, **BSP-1**, **BSP-2** and **BSP-3** were made. Excitation wavelengths were set as follows: 358 nm (**acTTh**), 362 nm (**cbTTh**), 360 nm (**BSP-2** and **BSP-3**). The solutions were stored in sealed volumetric flasks for 24 hrs under nitrogen in the dark. Photo-isomerisation to the relatives **MC-1**, **MC-2** and **MC-3** was carried out with *in situ* LED illumination (λ_{max} 375 nm) for 180 seconds.

Results and Discussion

Material synthesis

The synthesis of **BSP-3** in 77% yield by a base–catalyzed substitution of **BSP-1** onto **cbTTh** was straightforward and its spectral data (see Electronic Supplementary Information (ESI)) was consistent with this structure. As expected, its ^{1}H NMR spectrum was near identical to that of **BSP-2** except for the absence of the methylene signal at δ = 7.3.

Photochromic properties

It is well known that **MC** derivatives typically exhibit negative solvatochromism, meaning that the absorption maximum undergoes a hypsochromic (blue) shift as the solvent polarity increases, due to interactions between the solute and the solvent molecules that increase the energy gap between the **MC** ground and the excited states.[18-21,42] The focus of this study is whether the spectroscopic properties and switching behaviour of the **BSP** group is affected by attachment of the differing **TTh** sub-units.

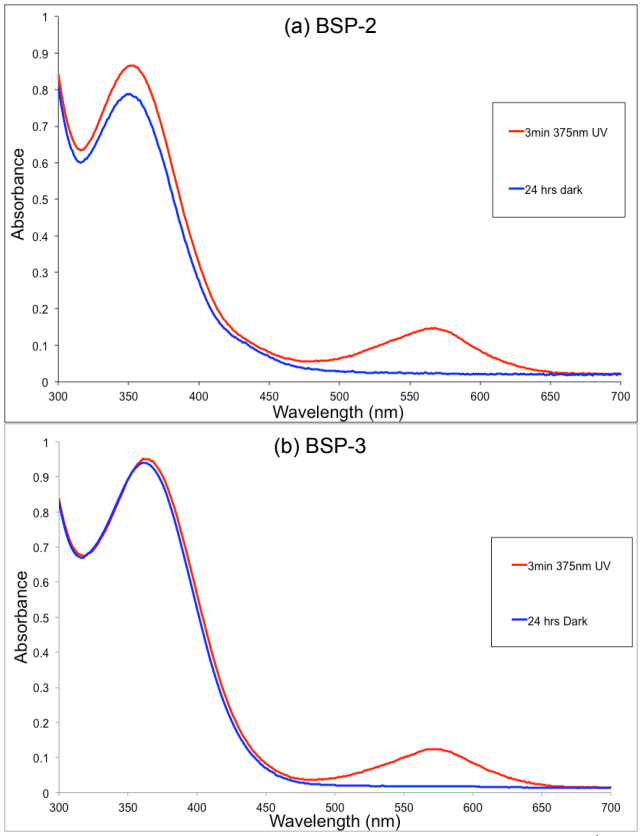

Fig. 3 Baseline corrected UV-*vis* spectra before and after illumination of 10^{-4} M solutions of (a) **BSP-2** with its **MC-2** absorption band at 568 nm and (b) **BSP-3** with its **MC-3** absorption band at 572 nm, using the 3 UV LED light source with λ_{max} emission = 375 nm; exposure time = 3 minutes.

UV-*vis* spectra of the two spiropyran-functionalised terthiophenes show two major absorbance bands with maxima at 352 nm and 362 nm for **BSP-2** and **BSP-3,** respectively (**TTh** absorbance, **BSP** contribution not shown[38]) and 568 nm and 572 nm for **MC-2** and **MC-3,** respectively (**MC** absorbance), as shown in Figure 3 (a) and (b). All solutions were kept in the dark for 24 hr at 293 K to establish thermodynamic equilibrium prior to UV illumination. In Figure 3 (a), the absorbance maximum at ca. 360 nm is greater for **MC-2** compared to **BSP-2**, whereas they are the same for **BSP-3** and **MC-3** (Figure 3 (b)). This suggests that there is a change in the electronic structure of **MC-2** relative to **BSP-2**, which does not occur with **BSP-3**/**MC-3**.

Kinetics of photo-induced ring opening

Figures 4 (a) and (b) show the spectra used to obtain the λ_{max} values for substitution into the model (equation 1), while Figure 4 (c) gives the growth in absorbance over time (293 K) at the λ_{max} for **MC-1**, **MC-2** and **MC-3** (spectra for **MC-1** are given in ESI, Figure S1). The ring opening process analysed using equation (1) occurs ~1.5 times faster for **BSP-2** compared to **BSP-3** (k_{BSP-2} = 4.45 x 10^{-4} s^{-1} versus k_{BSP-3} = 2.85 x 10^{-4} s^{-1}). For **BSP-1** the equivalent rate constant was higher again (k_{BSP-1} = 1.09 x 10^{-3} s^{-1}), giving an order in terms of speed of ring opening of **BSP-1 > BSP-2 > BSP-3.**

Extrapolation of the fitted curves using equation (1) allowed estimation of the steady state absorbance values for the derivatives in ACN. For the formation of **MC-2**, the model suggests the steady state (ca. 0.4 a.u.) is reached in about 150 minutes while for the formation of **MC-3** steady state absorbance is relatively constant at ca. 0.50 a.u. after about 200 min. This would be expected due to **BSP-2** having a faster ring-opening rate than **BSP-3** (Figure 4 (c)). Clearly, there is a significant difference in the steady state absorbance of **BSP-1** relative to **BSP-2** and **BSP-3**: the detected maximum absorbance for **BSP-1** after 45 minutes of exposure to the LED device was 1.84 a.u. at 563 nm *versus* 0.31 a.u. at 568 nm and 0.39 a.u. at 572 nm for **BSP-2** and **BSP-3**, respectively. This is most likely due to competing absorbance by the **TTh** moiety present in **BSP-2** and **BSP-3**, which reduces the availability of UV-photons for driving the ring-opening process.

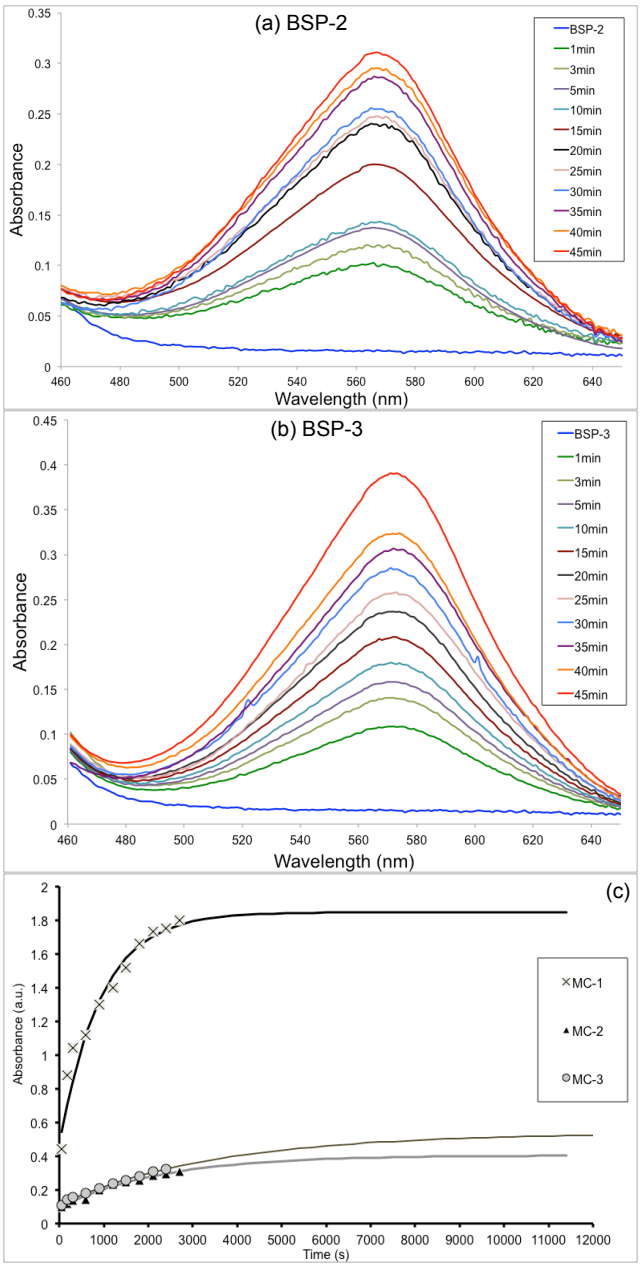

Fig. 4 Exposure effects to 375 nm UV LEDs: (a) Baseline corrected conversion of **BSP-2** (10^{-4} M in ACN) to the isomer **MC-2**. (b) Baseline corrected conversion of spiropyran **BSP-3** (10^{-4} M in ACN) to the isomer **MC-3**. (c) Exponential curves extrapolated to steady state for generation of **MC** isomers versus time of UV irradiation with experimental results superimposed for **MC-2** and **MC-3**. Values were taken at λ_{max} **MC-1** = 563 nm, **MC-2** = 568 nm, **MC-3** = 572 nm.

Further indications supporting this statement might be found by

comparing the ring opening of **BSP-2** and **BSP-3**. Extrapolation of the curves (Figure 4 (c)) suggests that the process reaches steady state after ca. 150 minutes for **MC-2** and ca. 200 minutes for **MC-3**. This model predicts final maximum absorbances for 10^{-4} M acetonitrile solutions of ca. 0.39 a.u. for **MC-2,** and ca. 0.5 a.u. for **MC-3**, considerably smaller if compared to derivatives already reported in literature for **BSP-1** (1.8 a.u.)[42]. The calculated rate of ring opening in the described process, **BSP→MC**, is fastest for **BSP-2** compared to **BSP-3**, but both are slower than **BSP-1** by an order of magnitude.

Kinetics and thermodynamics of ring closure

Table 1 shows the rate constants for ring closure (**MC→BSP**) over the temperature range 283 K – 308 K for **BSP-1**, **BSP-2** and **BSP-3**, and the ratios of the rate constants for each form. The **MC-3**/**MC-2** ratio steadily increases from 0.5 at 283 K to 1.4 at 308 K, meaning that at 283 K, **MC-2** relaxation is faster, whereas at 308 K, **MC-3** is faster. This pattern of behaviour is repeated for **MC-1** compared to **MC-2**, with the ratio = 0.42 at 283 K, increasing to 1.15 at 308 K. In contrast, the **MC-1**/**MC-3** ratio remains relatively constant over the temperature range studied, at about 0.8. These results suggest that the temperature affects ring closure kinetics in a similar manner for **BSP-3** compared to the parent **BSP-1** (increases around 3-fold), but a different type of dependency is observed with **BSP-2** (remains relatively constant). Furthermore, at 283 K **MC-2** reversion to **BSP-2** is the fastest for the three derivatives studied, whereas at 308 K, it is the slowest.

Table 1 Rate constants **k** and their ratios for **MC→BSP** thermal relaxation for **MC-1**, **MC-2** and **MC-3** (10^{-4} M in ACN) over 283 – 308 K averaged from 3 replicates. Standard deviations reported in brackets.

	λ_{max}	k ($10^{-3}s^{-1}$) in ACN					
	(nm)	283 K	288 K	293 K	298 K	303 K	308 K
MC-1	563	0.5 (±0.002)	1.06 (±0.001)	2.2 (±0.001)	4.5 (±0.0009)	9.04 (±0.0009)	18.3 (±0.0014)
MC-2	568	1.2 (±0.002)	2.6 (±0.002)	4.3 (±0.0009)	8.3 (±0.002)	11.7 (±0.008)	15.8 (±0.007)
MC-3	572	0.6 (±0.004)	1.5 (±0.002)	3.6 (±0.001)	5.9 (±0.001)	10.9 (±0.001)	21.6 (±0.002)
Ratios MC 1/2		0.42	0.40	0.50	0.52	0.77	1.15
Ratios MC 1/3		0.83	0.70	0.62	0.76	0.82	0.84
Ratios MC 3/2		0.50	0.57	0.69	0.71	0.93	1.36

Figure 5 shows the absorbance decrease at 568 nm for MC-3 in ACN (10^{-4} M) at different temperatures (similar spectra for **MC-2** and **MC-1** are given in the ESI, Figures S3 and S4, respectively), from which the rate constants for ring closing (thermal relaxation) at each temperature were obtained by fitting a first order rate equation.

The resulting Arrhenius and Eyring plots are shown in Figure 6 (a) and (b). From the Arrhenius plots, the activation energy (E_a) and the pre-exponential factor were derived (Table 2) for the thermal relaxation process. Using Eyring's transition state theory (Equation (4)), the activation thermodynamic parameters, $\Delta S^{\ddagger}$ (entropy of activation), $\Delta H^{\ddagger}$ (enthalpy of activation) and $\Delta G^{\ddagger}$ (Gibbs free energy of activation), for the thermal relaxation process can be estimated, (Table 2, Figure 6 (b)).

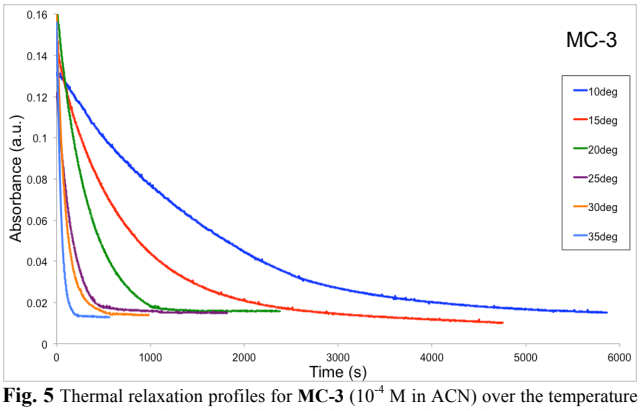

Fig. 5 Thermal relaxation profiles for **MC-3** (10^{-4} M in ACN) over the temperature range 283-308 K. Prior to acquisition of the spectra, the solutions were irradiated with the 3 UV-LED device (λ_{max} = 375 nm) for 180 s.

The Arrhenius and Eyring plots both show that **MC-1** and **MC-3** exhibit strikingly similar behaviour, with almost identical slopes, and a slight offset, whereas **MC-2** has a lower slope in both cases, with a higher rate constant at lower temperatures that gradually converges and eventually crosses the other plots. This pattern of behaviour is reflected in the values of the rate constants (Table 1) discussed above, and in the thermodynamic and kinetic parameters extracted from the Arrhenius and Eyring Plots (Table 2). Taking each in turn, analysis by Arrhenius theory returns an activation energy for **MC-2** that is ca. 25% lower (75.05 kJ mol^{-1} for **BSP-2** compared to 100.39 kJ mol^{-1} for **BSP-3**, and 101.49 kJ mol^{-1} for **BSP-1**), and a pre-exponential factor that is smaller by 4 orders of magnitude (ca. 10^{11} vs. 10^{15}); Eyring theory returns similar Gibb's free energy of activation (85-87 KJ mol^{-1}) and equilibrium constants of activation (ca. 4-7 $x10^{-16}$) in all three cases, but the entropy of activation ($\Delta S^{\ddagger}$) is negative for **MC-2** (-43.38 KJ mol^{-1}) and positive for **MC-3** (37.78 KJ mol^{-1}) and **MC-1** (46.48 KJ mol^{-1}). This quantity (for the process **MC→MC‡**) is related to the degree of order of the system as the **MC** molecules reorganise within the solvent system due to conformational changes as they pass into the transition state, **MC‡**. The negative value for **MC2→MC2‡** suggests that the formation of the transition state results in a more ordered system compared to the equivalent processes for **MC-1** and **MC-3**. Finally, the enthalpy of activation for **MC-2** is 73.05 KJ mol^{-1}, about 25% lower than the values for **MC-3** and **MC-1**. These data suggest that the difference in kinetics of ring closing observed for **MC-2** may arise primarily for entropic reasons, possibly due to differences in the conformation adopted by **MC-2**/**BSP-2** compared to the other derivatives.

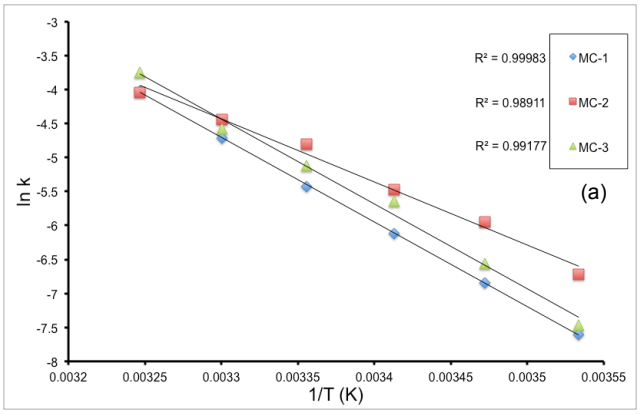

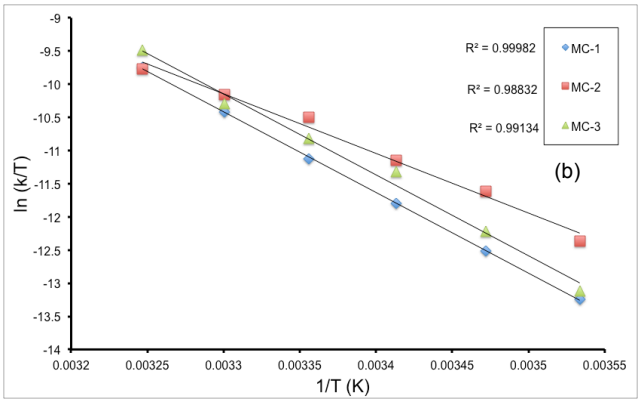

Fig. 6 Comparative (a) Arrhenius plots and (b) Eyring plots for the thermal relaxation process **MC→BSP**. All solution concentrations were 10^{-4} M in ACN. The values for **MC-2**, **MC-1** and **MC-3** were estimated from the thermal relaxation profiles in figures S-3, S-4 and Figure 5, respectively.

One explanation for these results is the additional methylene group in the **BSP-2** linker chain provides a degree of increased flexibility, and the two functional units (**BSP** and **TTh**) may be better able to align, for example, through intramolecular π-π interactions. This would be particularly so when the planar merocyanine isomer is present, and this would favour the adoption of a more ordered configuration, which is consistent with the negative value of $\Delta S^{\ddagger}$ for **BSP-2**.

This explanation is also supported by the difference in $\Delta H^{\ddagger}$ between the three spiropyrans; $\Delta H^{\ddagger}$ for **BSP-2** is ~20 kJ mol^{-1} lower than **BSP-1** and **BSP-3**. This suggests that the **MC-2** adopts a ground state conformation somewhat closer to the transition state leading to the spiropyran (**BSP-2**) than **MC-3** does on isomerising to **BSP-3**. Given that the formation of spiropyran from merocyanine typically requires rotation about the three bonds linking the indoline and phenolate components of the merocyanine, as discussed extensively by Wojtyk *et al.*[43], a π-π interaction between the terthiophene and the phenolate component of **MC-2** that brought the phenolate oxygen (in polar solvents) or quinone oxygen (in non-polar solvents) closer to the indoline nitrogen should lower $\Delta H^{\ddagger}$. Such an **MC** conformation could be determined by π-π interactions during the ring opening of the spiropyran to form the merocyanine initially.

Table 2 Thermodynamic parameters expressed as a mean of 3 replicates and standard deviation (standard deviations values are reported in brackets) for **MC-2** ⇌ **BSP-2** and **MC-3** ⇌ **BSP-3** thermal relaxation compared to the results obtained from a reference solution of **BSP-1** 10^{-4} M in ACN.

			Arrhenius		Eyring			
MC	λ_{max} (nm)	k_{293} (10^{-3} s^{-1})	**Ea** (kJ mol^{-1})	**A** (s^{-1})	$\Delta S^{\ddagger}$ (JK^{-1} mol^{-1})	$\Delta G^{\ddagger}_{293}$ (kJ mol^{-1})	$\Delta H^{\ddagger}$ (kJ mol^{-1})	$K^{\ddagger}_{293}$ (10^{-16})
MC-1	563	2.2	101.49 (±2.06)	3.51 x 10^{15} (±2.83)	46.48 (±2.92)	86.59 (±0.082)	99.04 (±2.06)	3.56 (±0.108)
MC-2	568	4.3	75.05 (± 1.5)	1.35 x 10^{11} (± 0.9)	-43.38 (± 2.07)	85.17 (± 0.18)	73.05 (± 1.5)	6.57 (± 0.73)
MC-3	572	3.6	100.39 (± 3.06)	8.62 x 10^{15} (± 0.24)	37.78 (± 2.81)	85.94 (± 0.23)	96.74 (± 1.42)	5.93 (± 0.74)

Solvatochromic effects

Samples of **BSP-2** and **BSP-3** were dissolved in selected solvents and kept in the dark for 24 hr before solvatochromic studies were carried out. For this study, a polar protic solvent (ethanol) and polar aprotic solvents (acetone, acetonitrile) were used and their effect compared to non-polar solvents (toluene, dichloromethane and diethyl ether). Figure 7 shows spectra obtained for **MC-3** in a number of solvents after irradiation for 180 seconds with UV light (375 nm), along with inset photographs of the resulting solutions. In addition, the thermal relaxation rate constants were estimated at 293 K (Figures 8 (a) and (b), extrapolated from Figure S2 (a) and (b), ESI) in each solvent. The formation of J-aggregates (Figure 7) in non-polar solvents typical of many **BSP** derivatives is evident from the appearance of new absorbance bands at 605 nm and 599 nm for **MC-3**, and at 605 nm and 597 nm for **MC-2** (Figure S5, ESI), in toluene and diethyl ether, respectively.

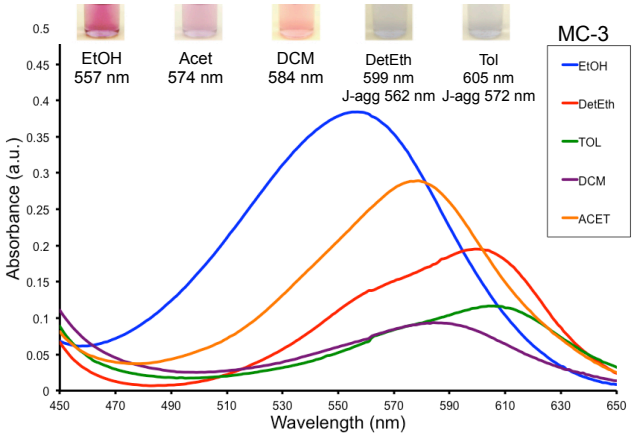

Fig. 7 Solvatochromic effects of **MC-3** in the following solvents: EtOH, Acet, DCM, DetEth and Tol, listed and inset in terms of decreasing polarity. Prior to acquisition of the spectra, the solutions were irradiated with UV-LED device (λ_{max} = 375 nm) for 180 s at 293 K. [**BSP-3**] = 10^{-4} M in all cases.

Table 3 shows clearly that for both **MC-2** and **MC-3**, the λ_{max} is blue-shifted as the solvent polarity increases (negative solvatochromism) from toluene through to ethanol (605 nm to 552 nm for **MC-2**, 552 nm to 557 nm for **MC-3**). As is well established in the literature, merocyanines exhibit negative solvatochromism as a result of both a decrease in the dipole moment on electronic excitation and an increase in the dipolar nature of the ground state.[43] It has also been shown that this tends

to be independent of the nature of the N-substituent, and this is indeed the case for **MC-2** and **MC-3**, which show near identical solvatochromic behaviour.

In contrast, the rate constant for ring closure (k) decreases by an order of magnitude from 24.3 x 10^{-3} s^{-1} to 2.4 x 10^{-3} s^{-1} for **MC-2** for increasing solvent polarity, while for **MC-3** an even greater rate decrease occurs (25.7 x 10^{-3} s^{-1} to 0.7 x 10^{-3} s^{-1}). The values for the rate constants for ring closure are similar in acetonitrile, acetone, diethyl ether and toluene, implying that solvation of the **MC** isomers must be quite similar. However, in ethanol this is not the case, as ring closure is four times faster for **MC-2**.

Table 3 Photo and thermal properties of **MC-2** and **MC-3** derivatives (10^{-4} M) in a selection of solvents. λ_{max} measured after 15 hrs in the dark. The thermal relaxation rate constants were calculated by plotting ln k vs. time, where k = slope.

SOLVENT	MC-2			MC-3		
	λ_{max} nm	Abs	k ($10^{-3}s^{-1}$)	λ_{max} nm	Abs	k ($10^{-3}s^{-1}$)
Ethanol	552	0.42	2.4	557	0.3	0.7
Acetonitrile	568	0.12	4.3	572	0.1	3.6
Acetone	570	0.44	6.3	574	0.4	6.3
Dichloromethane	587	0.13	9.2	584	0.4	17.3
Diethyl ether	597	0.29	21.9	599	0.2	19.3
Toluene	605	0.42	24.3	605	0.5	25.7

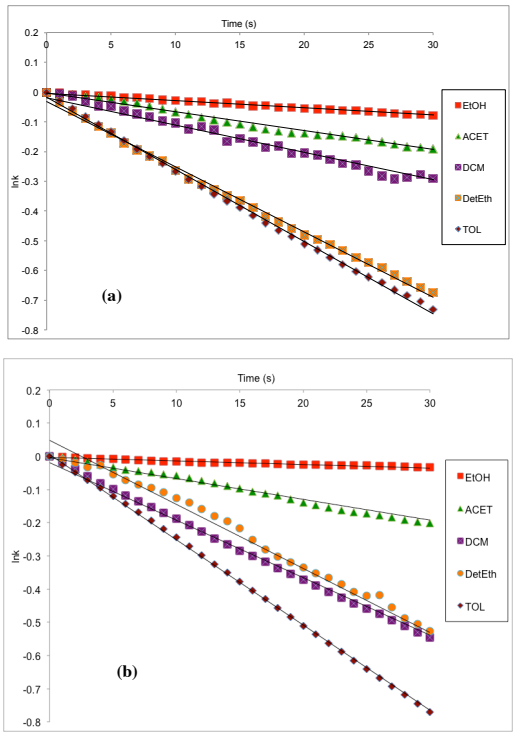

Fig. 8 The ln k vs. time plots used to calculate the rate of thermal relaxation of 10^{-4} M solutions of **BSP-2** (a) and **BSP-3** (b) in common organic solvents at 293 K.

This implies that, even though the dipolar nature of the **MC-2** ground state is similar to that of **MC-3** (similar λ_{max} values), the ethanol is acting like a less polar solvent with regard to ring closure rate. If intramolecular p-p interactions do indeed control the ground state conformation of **MC-2**, then **MC-2** is in effect partly solvated by the p bonds of terthiophene, a less polar "solvent", diminishing the full effect of the polar ethanol solvent. Somewhat more surprising is the contrary effect of dichloromethane for which ring closure is almost twice as fast for **MC-3** relative to **MC-2**, even though they appear to be electronically similar in this solvent. A more detailed study needs to be undertaken to probe the reasons for this behaviour.

Fluorescence spectroscopy

The presence of intramolecular π-π interactions in **MC-2** would be expected to have a significant impact on the emissive properties of the molecule. The emissions of the terthiophene components of both **BSP-2** and **BSP-3** and their corresponding merocyanines were investigated since excitation of the molecules at 360 nm would lead to typical terthiophene emissions[26] around 450 nm that overlapped with the edge of the merocyanine absorptions (Figure 3). The corresponding emission spectra, as well as those of **BSP-1**/**MC-1** and the terthiophene acids are presented in Figure 9 (a) and (b), and the relevant data given in Table 4. A comparison of the emission spectra of the two terthiophenes shows, as expected, that **acTTh** is blue shifted by 28 nm (Figure 9 (a), $\lambda_{max,em}$ = 439 nm) compared to **cbTTh** (Figure 9 (b), $\lambda_{max,em}$ = 467 nm as a result of the effect of the loss of conjugation of the carboxylic acid. However, both **BSP-2** ($\lambda_{max,em}$ = 464 nm) and **MC-2** have notably red-shifted (~25 nm) terthiophene emissions (Figure 9 (a) and Table 4) whilst those of **BSP-3** and **MC-3** are largely unchanged (Figure 9 (b) and Table 4).

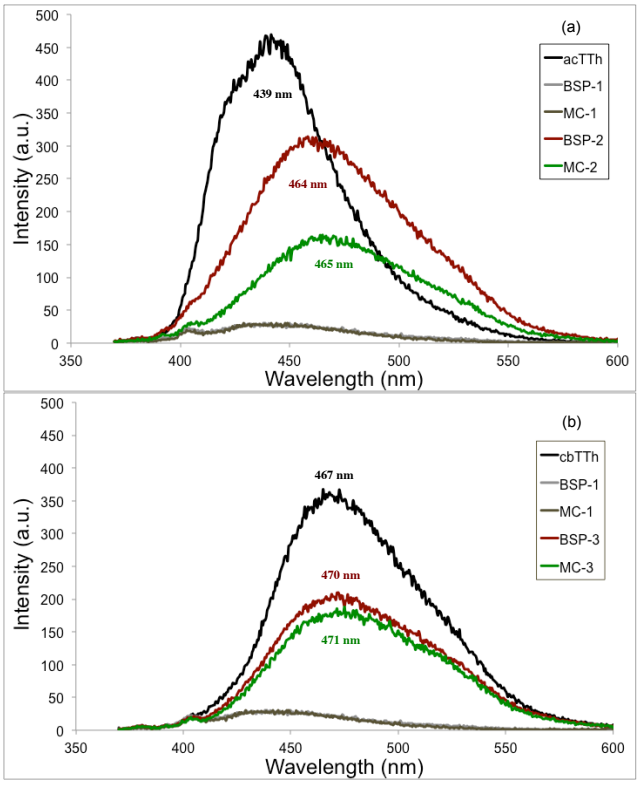

Fig. 9 (a) Emission spectra of **acTTh**, **BSP-1**, **BSP-2** and their related **MC** isomers. (b) Emission spectra of **cbTTh**, **BSP-1**, **BSP-3** and their related **MC** isomers. All the solutions were 10^{-5} M in ACN and all excitation wavelengths were 360 nm.

Clearly, there is a much larger structural effect on the emission properties of **BSP-2** and **MC-2** than can be accounted for by a single carbon atom, and this is fully consistent with the influence of intramolecular π-π interactions. However, it should be noted that since the emission shift is similar for both **BSP-2** and **MC-2**, similar interactions must be present in both isomers.

Table 4 Parameters derived from the analysis of the emission spectra of **acTTh**, **cbTTh**, **BSP-2** and **BSP-3**. Stokes shifts are also indicated.

Molecules	λ_{max} UV-*vis* cm^{-1} (nm)	λ Excitation (nm)	λ_{max} Emission cm^{-1} (nm)	Stokes Shift cm^{-1}
acTTh	28,090 (356)	358	22,727 (440)	5363
cbTTh	27,472 (364)	362	21,413 (467)	5874
BSP-2	28,090 (356)	360	21,598 (463)	6492
BSP-3	27,472 (364)	360	21,276 (470)	6196

Equally significant in this regard is the change in emission intensity for the **BSP-2/MC-2** isomers, which is absent for **BSP-3/MC-3**. While the quantum yields of the molecules were not measured and therefore, it is difficult to draw any conclusions from the relative intensities of the two sets of molecules, the apparent quenching of the **MC-2** terthiophene emission is again consistent with a intramolecular π-π interaction between the planar merocyanine moiety and the terthiophene. This may also explain the increase in the merocyanine absorbance at 355 nm (Figure 3 (a)) when **BSP-2** is exposed to UV light, which does not manifest when the same experiment is performed with **BSP-3,** suggesting that a new interaction occurs when **BSP-2** is switched to **MC-2**.

Therefore, these results suggest that the extra methylene group present in the **BSP-2** linker chain provides a degree of additional flexibility that leads to enhanced intramolecular interaction between the **MC** and **TTh** units, most likely through alignment of π-electrons, as the molecule folds around the linker chain. A 3-d representation of this intramolecular alignment of the **MC** and **TTh** π-electrons is shown in Figure 10 (a) and (b)). . This was produced by generating the energy minimised **MC** and **TTh** sub units in Chem-3D Ultra using standard molecular mechanics and arranging these with the appropriate linker chain, while applying typical constraints for the various bond lengths and angles. This tentatively suggests that is possible for the sub-units to align, with a separation as close as 3-5-3.7Å, which is well within the range for π-stacking. As indicated by the shift in the emission spectra, such an interaction is also likely between the **BSP** and **TTh** moieties in **BSP-2**, although perhaps not as strongly given the non-planar nature of the **BSP** unit. In the case of **BSP-3/MC-3**, the shorter linker group, coupled with the extended conjugation of the **TTh**-π electrons into the carbonyl group prevents this interaction from occurring and the fluorescence and absorbance spectra are not affected in the same manner. A more rigorous *ab initio* study using molecular orbital theory calculations is currently underway and will be the subject of a separate publication.

This explanation is also consistent with the observed differences in the kinetic and thermodynamic behaviour of the **BSP-2** and **BSP-3**. For example, **BSP-3** is similar to **BSP-1** in terms of thermal relaxation behaviour. Table 1 shows that the ratio of the rate constants remains virtually constant over the temperature range studied (283 K-308 K), whereas for **BSP-2**, the ratio increases markedly towards the higher end of the range. This could be explained in terms of disruption of the **MC** and **TTh** π-electron alignment as the system energy increases. Similar explanations have been advanced for observed patterns in the kinetics the thermal relaxation of the merocyanine form of spironaphtooxazine derivatives.[44]

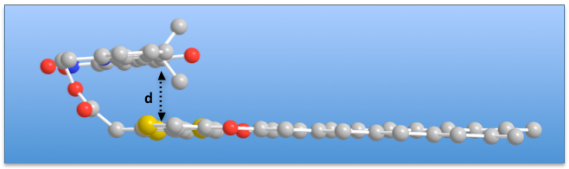

(a)

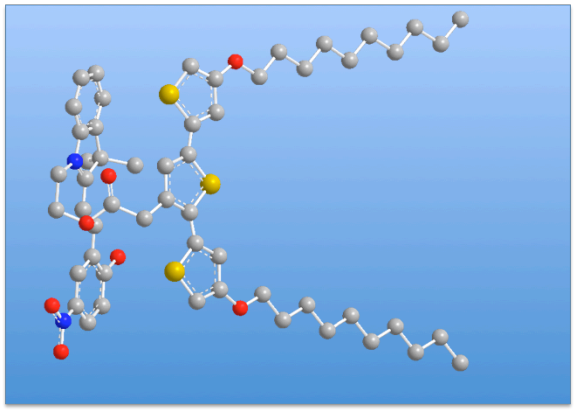

(b)

Fig. 10 (a) Side view of **MC-2** in a 'U' arrangement showing the distance 'd' (3-5-3.7Å) between the aligned **MC** and **TTh** moieties and (b) alternative view of the same arrangement of the **MC** and **TTh** moieties. Images generated using Chem-3d Ultra V10.0 . Atom types carbon (grey), oxygen (red), nitrogen (blue), sulphur (yellow); hydrogen atoms not displayed for clarity.

Conclusions

The photochemical and thermodynamic properties of two derivatives, **BSP-2** and **BSP-3**, incorporating terthiophene units attached to spiropyrans via the indoline nitrogen atom and ester linkers that differ by one methlyene unit have been investigated. In **BSP-2**, the pyran is separated from the ester group by a methylene group, whereas in **BSP-3**, the ester group is directly linked to the terthiophene group. This apparently rather small structural difference results in quite striking differences in the characteristics of the derivatives, such as the fluorescence emission spectra (dominated by the terthiophene unit) and the thermal relaxation kinetics of the spiropyran unit. We believe these differences arise from the ability of the π-electron clouds of the thiophene and spiropyran units to align and form intramolecular π-π interactions in **BSP-2** due to the flexibility of the longer linker chain. In **BSP-3**, the terthiophene conjugation extends into the ester group of the linker, and this additional rigidity, coupled with the shorter linker length, prevents a similar type of interaction from occurring. We are now developing a new generation of polymers based on these derivatives that could exploit such effects.

Acknowledgements

MZ, RB and DD acknowledge funding from Science Foundation Ireland (SFI) under the CLARITY CSET award (Grant 07/CE/I1147). KJF acknowledges the European Commission for financial support through a Marie Curie Actions International Re-integration Grant (IRG) (PIRG07-GA-2010-268365) and Irish Research Council for Science, Engineering and Technology. We also acknowledge support from the European Commision for funding under grant PIRSES-GA-2010-269302.

Financial support from the Australian Research Council and access to the Australian National Fabrication Facility are also gratefully acknowledged.

[a] *CLARITY: Centre for Sensor Web Technologies, National Centre for Sensor Research, Dublin City University, Dublin 9, Ireland. E-mail: dermot.diamond@dcu.ie; Fax: +353 1 700 7995; Tel: +353 1 700 5404.*

[b] *ARC Centre of Excellence for Electromaterials Science and Intelligent Polymer Research Institute, University of Wollongong, Northfields Avenue, Wollongong, NSW 2522, Australia.*

† Electronic Supplementary Information (ESI) available: Characterization of **BSP-3**. Baseline corrected conversion of **BSP-1** (10^{-4} M in ACN) to the isomer **MC-1**. Thermal relaxation profiles of synthesized **MC-2** and **MC-3** in various solvents. Thermal relaxation profile of **MC-1** and **MC-3** in ACN at various temperatures. Solvatochromic effect of a range of solvents on **BSP-2**. See DOI: 10.1039/b000000x/.

References

1. Y. Hirshberg, *Journal of the American Chemical Society*, 1956, **78**, 2304-2312.
2. E. Berman, R. E. Fox and F. D. Thomson, *Journal of the American Chemical Society*, 1959, **81**, 5605-5608.
3. C. A. Heller, D. A. Fine and R. A. Henry, *The Journal of Physical Chemistry*, 1961, **65**, 1908-1909.
4. J. G. Calvert and J. N. J. Pitts, *Photochemistry*, John Wiley and Sons, Inc., New York, N.Y., 1966.
5. R. Guglielmetti, *Studies in Organic Chemistry*, 1990, **40**, 855-879.
6. V. I. Minkin, *Chemical Reviews*, 2004, **104**, 2751-2776.
7. T. Yoshida and A. Morinaka, *Journal of Photochemistry and Photobiology a-Chemistry*, 1994, **78**, 179-183.
8. I. Willner, S. Rubin and Y. Cohen, *Journal of the American Chemical Society*, 1993, **115**, 4937-4938.
9. J. C. Crano, T. Flood, D. Knowles, A. Kumar and B. VanGemert, *Pure and Applied Chemistry*, 1996, **68**, 1395-1398.
10. S. Stitzel, R. Byrne and D. Diamond, *Journal of Materials Science*, 2006, **41**, 5841-5844.
11. F. Benito-Lopez, R. Byrne, A. M. Răduță, N. E. Vrana, G. McGuinness and D. Diamond, *Lab on a Chip*, 2010, **10**, 195.
12. A. S. Dvornikov, J. Malkin and P. M. Rentzepis, *Journal of Physical Chemistry*, 1994, **98**, 6746-6752.
13. H. Bouas-Laurent and H. Dvorr, in *Photochromism*, eds. D. r. Heinz and B.-L. Henri, Elsevier Science, Amsterdam, 2003, pp. XXVII-LIII.
14. R. Byrne, K. J. Fraser, E. Izgorodina, D. R. MacFarlane, M. Forsyth and D. Diamond, *Physical Chemistry Chemical Physics*, 2008, **10**, 5919-5924.
15. S. Coleman, R. Byrne, S. Minkovska and D. Diamond, *Journal of Physical Chemistry B*, 2009, **113**, 15589-15596.
16. R. Byrne, S. Coleman, K. J. Fraser, A. Raduta, D. R. MacFarlane and D. Diamond, *Physical Chemistry Chemical Physics*, 2009, **11**, 7286-7291.
17. R. Byrne, S. Coleman, S. Gallagher and D. Diamond, *Physical Chemistry Chemical Physics*, 2010, **12**, 1895-1904.
18. A. K. Chibisov and H. Gorner, *Chemical Physics*, 1998, **237**, 425-442.
19. H. Gorner, *Chemical Physics Letters*, 1998, **288**, 589-589.
20. H. Gorner, *Physical Chemistry Chemical Physics*, 2001, **3**, 416-423.
21. H. Gorner and A. K. Chibisov, *Journal of the Chemical Society-Faraday Transactions*, 1998, **94**, 2557-2564.
22. K. J. Laidler and J. H. Meiser, *Physical Chemistry* Houghton Mifflin, Boston, MA, 1999.
23. J. Roncali, *Chemical Reviews*, 1992, **92**, 711-738.
24. J. Roncali, *Chemical Reviews*, 1997, **97**, 173-205.
25. S. Gambhir, K. Wagner and D. L. Officer, *Synthetic Metals*, 2005, **154**, 117-120.
26. P. Wagner and D. L. Officer, *Synthetic Metals*, 2005, **154**, 325-328.
27. M. C. Gallazzi, L. Castellani, R. A. Marin and G. Zerbi, *Journal of Polymer Science Part a-Polymer Chemistry*, 1993, **31**, 3339-3349.
28. C. H. E. Zhou, Z. Tan, C. Yang, Y. Li, *Journal of Polymer Science Part B*, 2006, **44**, 4916-4922.
29. S. H. Hosseini and A. A. Entezami, *Polymers for Advanced Technologies*, 2001, **12**, 524-534.
30. L. Kumpumbu-Kalemba and M. Leclerc, *Chemical Communications*, 2000, 1847-1848.
31. I. Levesque, P. Bazinet and J. Roovers, *Macromolecules*, 2000, **33**, 2952-2957.
32. I. Levesque and M. Leclerc, *Chemistry of Materials*, 1996, **8**, 2843-2849.
33. I. Levesque and M. Leclerc, *Macromolecules*, 1997, **30**, 4347-4352.
34. F. Raymond, N. Di Cesare, M. Belletete, G. Durocher and M. Leclerc, *Advanced Materials*, 1998, **10**, 599-602.
35. A. Yassar, C. Moustrou, H. K. Youssoufi, A. Samat, R. Guglielmetti and F. Garnier, *Macromolecules*, 1995, **28**, 4548-4553.
36. K. Yoshino, S. Nakajima, M. Onoda and R. Sugimoto, *Synthetic Metals*, 1989, **28**, 349-357.
37. G. Zotti, R. A. Marin and M. C. Gallazzi, *Chemistry of Materials*, 1997, **9**, 2945-2950.
38. K. Wagner, R. Byrne, M. Zanoni, S. Gambhir, L. Dennany, R. Breukers, M. Higgins, P. Wagner, D. Diamond, G. G. Wallace and D. L. Officer, *Journal of the American Chemical Society*, 2011, **133**, 5453-5462.
39. A. Higuchi, A. Hamamura, Y. Shindo, H. Kitamura, B. O. Yoon, T. Mori, T. Uyama and A. Umezawa, *Biomacromolecules*, 2004, **5**, 1770-1774.
40. J. M. Locke, S. Gambhir, R. D. Breukers, K. Wagner, K. W. Jolley, G. G. Wallace and D. L. Officer, *Manuscript in preparation.*, 2012.
41. D. Diamond and V. C. A. Hanratty, *Spreadsheet Applications for Chemistry Using Microsoft Excel*, John Wiley and Sons, New York, 1997.
42. J. B. Flannery, *Journal of the American Chemical Society*, 1968, **90**, 5660-5671.
43. J. T. C. Wojtyk, A. Wasey, P. M. Kazmaier, S. Hoz and E. Buncel, *The Journal of Physical Chemistry A*, 2000, **104**, 9046-9055.
44. T. W. Shin, Y. S. Cho, Y. D. Huh, K. D. Lee, W. K. Yang, J. Park and I. J. Lee, *Journal of Photochemistry and Photobiology a-Chemistry*, 2000, **137**, 163-168.